

Abstract

A distinct, subsurface density front along the eastern St. Anna Trough in the northern Kara Sea is inferred from hydrographic observations in 1996 and 2008–2010. Direct velocity measurements show a persistent northward subsurface current ($\sim 20 \text{ cm s}^{-1}$) along the St. Anna Trough eastern flank. This sheared flow, carrying the outflow from the Barents and Kara Seas to the Arctic Ocean, is also evident from shipboard observations as well as from geostrophic velocities and numerical model simulations. Although no clear evidence for the occurrence of shear instabilities could be obtained, we speculate that the enhanced vertical mixing along the St. Anna Trough eastern flank promoted by a vertical velocity shear favors the upward heat loss from the intermediate warm Atlantic water layer. The associated upward heat flux is inferred to $50\text{--}100 \text{ W m}^{-2}$ using hydrographic data and model simulations. The zone of lowered sea ice thickness and concentration essentially marks the Atlantic water pathway in the St. Anna Trough and adjacent Nansen Basin continental margin from both sea-ice remote sensing observations and model simulations. In fact, the seaice shows a consistently delayed freeze-up onset during fall and a reduction in the seaice thickness during winter. This is consistent with our results on the enhanced Atlantic water heat loss along the Atlantic water pathway in the St. Anna Trough.¹

1 Introduction

The warm Atlantic water (AW) plays a role in reducing the sea-ice cover in the Northern Hemisphere through upward heat loss (Polyakov et al., 2010). The AW heat loss impacts the ice cover along the Arctic Ocean Eurasian continental margins (Polyakov et al., 2010), but is significantly stronger over the regions of the AW inflow into the Arctic Ocean through the Fram Strait (the Fram Strait branch of AW inflow – FSBW) and in the

¹Dedicated to the memory of our colleague Klaus Hochheim who tragically lost his life in the Arctic expedition in September 2013

OSD

11, 543–573, 2014

Heat loss from the Atlantic water layer

I. A. Dmitrenko et al.

Title Page

Abstract

Introduction

Conclusions

References

Tables

Figures

◀

▶

◀

▶

Back

Close

Full Screen / Esc

Printer-friendly Version

Interactive Discussion



Heat loss from the Atlantic water layer

I. A. Dmitrenko et al.

Title Page

Abstract

Introduction

Conclusions

References

Tables

Figures

◀

▶

◀

▶

Back

Close

Full Screen / Esc

Printer-friendly Version

Interactive Discussion



Barents Sea (the Barents Sea branch of AW inflow – BSBW). These are areas where the inflowing AW with temperatures $T \sim 5^\circ\text{C}$ occupies the surface layer directly affecting the ocean–sea ice–atmosphere interface (Sirevaag and Fer, 2009; Årthun et al., 2012; Ivanov et al., 2012). While transiting along the continental slope of Svalbard (red arrows in Fig. 1) and through the Barents Sea (blue arrows in Fig. 1), the AW gradually cools and deepens, getting isolated from the surface. In the area of the St. Anna Trough (hereinafter SAT) in the northern Kara Sea, the submerged BSBW with temperatures slightly above 0°C merges with a fraction of the warm intermediate FSBW ($T \sim 2.0\text{--}2.5^\circ\text{C}$) that enters the western SAT steered by the topography (Hanzlick and Aagaard, 1980; Schauer et al., 2002a) – Figs. 1 and 2. Hereafter we refer to this fraction of the FSBW as SAT-circulating FSBW (SFSBW).

The SFSBW return flow to the Arctic Ocean along the SAT eastern slope is colder and less saline than the FSBW (Schauer et al., 2002b), which indicates mixing and heat loss along the SFSBW pathway in the SAT as suggested by Hanzlick and Aagaard (1980). This allows speculations that a fraction of the SFSBW heat is released upwards with potential implication for the ocean–seaice–atmosphere interface. This paper addresses the issue of SFSBW modification in the SAT with a special focus on water dynamics and mixing occurring along the SAT eastern flank. We suggest that vertical mixing promoted by interaction of the SFSBW with Barents and Kara seas outflow can favor an enhanced AW heat loss that results in a consistent delay of freeze-up onset in fall, seaice thinning in winter, and earlier spring retreat.

2 Data and methods

Oceanographic CTD transects across the SAT (Fig. 2) were taken from the icebreaker *Kapitan Dranitsyn* along $\sim 81^\circ\text{N}$ (24 October 2008) and along $\sim 81^\circ\text{N}$ and 82°N (22–23 August 2009 and 2–3 September 2009, respectively), and from the R/V *Nikolay Evgenov* along $\sim 81^\circ\text{N}$ (22 September 2010). These sections were sampled using a shipboard SBE19+ CTD (2009–2010), Lockheed Martin Sippican Expendable

Heat loss from the Atlantic water layer

I. A. Dmitrenko et al.

Title Page

Abstract

Introduction

Conclusions

References

Tables

Figures

◀

▶

◀

▶

Back

Close

Full Screen / Esc

Printer-friendly Version

Interactive Discussion



Bathythermographs – XBTs and Expendable Conductivity, Temperature, and Depth Profilers – XCTDs (2008). These data were complemented by oceanographic stations occupied across the SAT along $\sim 82^\circ$ N in July 1996 during the ARKXII cruise of the RV *Polarstern* (Schauer et al., 2002b). In addition, we used the velocity data collected from a conventional mooring equipped with Teledyne RD Instruments 300 kHz Workhorse Sentinel Acoustic Doppler Current Profilers (ADCPs) measuring velocity through the depth range of 134–218 m and 376–468 m from 24 August 2009 to 22 September 2010. The mooring was deployed at the eastern slope of the SAT at $81^\circ 01' \text{ N}$, $73^\circ 02' \text{ E}$ (Fig. 2) in ~ 520 m water depth.

We use gridded satellite data of ice concentration (from the Integrated Climate Data Center at the University of Hamburg, Germany), ice thickness (from the Jet Propulsion Laboratory, USA), and ice drift (from the Center IFREMER of Brest, France). The seaice concentration is derived from the Advanced Microwave Scanning Radiometer for EOS - AMSR-E (2005–2010) and Special Sensor Microwave Imager/Sounder – SS-MIS (2011) (Spreen et al., 2008). The seaice thickness is from the Ice, Cloud, and land Elevation Satellite (ICESat) (Kwok et al., 2009). The sea-ice drift is from the 89 GHz brightness temperature of the AMSR (Ezraty et al., 2007). The spatial grid resolution for ice concentration, thickness and drift is 6.25 km, 25 km and 31.25 km, respectively. The surface level air temperature for the SAT area is from the National Centers for Environmental Prediction (NCEP) reanalysis (Kalnay et al., 1996).

In this study we use ocean velocity, seaice thickness and concentration, and vertical heat fluxes simulated with the coupled ocean–sea ice MIT general circulation model (Marshall et al., 1997). The model has been configured for the Atlantic region north of 30° S including the Nordic Seas and the Arctic Ocean. The model has 50 levels in the vertical, with resolution varying from 10 m in the upper ocean to 550 m in the deep ocean. It was initialized from rest and with the annual mean temperature and salinity from the World Ocean Atlas (WOA) 2005 monthly climatology (Boyer et al., 2005). Bottom topography was interpolated from the ETOPO2 database.

Heat loss from the Atlantic water layer

I. A. Dmitrenko et al.

Title Page

Abstract

Introduction

Conclusions

References

Tables

Figures

◀

▶

◀

▶

Back

Close

Full Screen / Esc

Printer-friendly Version

Interactive Discussion



The model was forced at the surface by fluxes of momentum, heat and freshwater computed using bulk formulae and the 1948–2010 6 hourly atmospheric state from the NCEP RA1 reanalysis (Kalnay et al., 1996). At the southern open boundary the model was forced by a 1° resolution global model solution and at Bering Strait a barotropic net inflow of 0.9 Sv was prescribed. The model sea surface salinity was relaxed to the WOA2005 monthly climatology to prevent long-term drifts. In the area of interest, the Barents and Kara Seas including the SAT, the horizontal resolution is 7 km.

The vertical mixing parameterization follows the K-Profile Parameterization (KPP) formulation by Large et al. (1994). Background coefficients of vertical diffusion and viscosity are both $1 \times 10^{-5} \text{m}^2 \text{s}^{-1}$. Biharmonic diffusion and viscosity represent unresolved eddy mixing, both with coefficients of $5 \times 10^9 \text{m}^4 \text{s}^{-1}$. For further details on the model set-up and application see (Serra et al., 2010).

The model is capable in realistic reproducing of the AW inflow into the Arctic Ocean through the Barents Sea Opening (BSO) and Fram Strait. The vertical structure of temperature and velocity at BSO (Fig. 3a) is in overall agreement with that shown in Skagseth (2008). The AW and the Bear Island Trough outflow temperatures (Fig. 3c) are also consistent with observations. Furthermore, the simulated volume transport of AW (defined as $T > 3^\circ\text{C}$) of about 1.7 Sv (Figs. 1 and 3e) agrees well with the 1.8 Sv value given in (Skagseth et al., 2008).

In the Fram Strait, the model performs reasonably well in terms of the vertical structure of mean temperature and velocity (Fig. 3b). The West Spitzbergen Current (WSC) has a realistic structure and the temperature of the AW (defined as $T > 2^\circ\text{C}$ – Fig. 3d) is in agreement with the time series presented in Beszczynska-Moeller et al. (2012). The long-term mean (1997–2009) simulated volume transport of AW in the core of the WSC at Fram Strait of about 1.4 Sv is directly comparable with the 1.3 Sv presented in Beszczynska-Moeller et al. (2012) based on measurements by an array of moorings in Fram Strait over the period 1998–2010 (Figs. 1 and 3f).

The model's ability to adequately simulate the AW dynamics, and thus to elaborate the relationships between the AW dynamics and ice conditions over the SAT region

($T_{\max} = 2.74^{\circ}\text{C}$) in the central part of the SAT mouth at 82°N (st. 80, Figs. 2 and 4b) exceeds those of the inflowing SFSBW by $0.2\text{--}0.4^{\circ}\text{C}$.

The observations in 1996 and 2008–2010 consistently show denser water at the eastern flank of the SAT below the halocline layer deeper than 50 m (Fig. 5). In 1996 over the SAT eastern flank shallower than ~ 300 m, the density front extended throughout the water column (Fig. 5a). At 150 m, the potential density gradient across the eastern flank along 81°N ranged from $0.09 \times 10^{-2} \text{ kg m}^{-3} \text{ km}^{-1}$ in 2010 (Fig. 5d) to $0.18 \times 10^{-2} \text{ kg m}^{-3} \text{ km}^{-1}$ in 2008–2009 (Fig. 5b and c). At 300 m, the cross-slope density gradient in 2008–2010 was more uniform with $\sim 0.16\text{--}0.18 \times 10^{-2} \text{ kg m}^{-3} \text{ km}^{-1}$ (Fig. 5b–d). For comparison, in 1996 the density gradient across the eastern flank was $\sim 0.22 \times 10^{-2} \text{ kg m}^{-3} \text{ km}^{-1}$ and $0.09 \times 10^{-2} \text{ kg m}^{-3} \text{ km}^{-1}$, at 150 m and 300 m, respectively (Fig. 5a). Moreover, in 1996 the surface layer is denser (saltier) and consequently the surface layer stratification is weaker (Fig. 5a).

The mean velocity profile derived from the 2009–2010 yr-long ADCP velocity measurements at the eastern flank shows a relatively stable, nearly barotropic northward flow aligned to $\sim 2^{\circ}$ in 140–220 m and to $\sim 11^{\circ}$ in 380–460 m, which is consistent with the orientation of the SAT eastern flank. The flow magnitude slightly increases with depth from $17 \pm 7 \text{ cm s}^{-1}$ at 140 m (Fig. 6b) to $20 \pm 7 \text{ cm s}^{-1}$ at 200 m, $21 \pm 5 \text{ cm s}^{-1}$ at 380 m, and $23 \pm 5 \text{ cm s}^{-1}$ at 460 m (not shown). This is in agreement with the shipboard ADCP observations in 1996 showing the northward sub-surface flow of $\sim 25\text{--}30 \text{ cm s}^{-1}$ (Fig. 6b, see Schauer et al., 2002a, for more details). In addition, the velocity profile in Fig. 6b demonstrates a velocity difference of $\sim 20 \text{ cm s}^{-1}$ in the upper 90 m. The sheared flow is also evident from the geostrophic velocity profiles at the mooring position in the SAT eastern flank derived from dynamic heights relative to the 0-dbar pressure surface using the potential density profiles from the nearest CTD stations (Figs. 5 and 6a). The simulated velocities also demonstrate a northward sheared flow along the SAT eastern flank, but twice as large as the geostrophical velocities (Figs. 6c, d, and 7).

Heat loss from the Atlantic water layer

I. A. Dmitrenko et al.

Title Page

Abstract

Introduction

Conclusions

References

Tables

Figures

◀

▶

◀

▶

Back

Close

Full Screen / Esc

Printer-friendly Version

Interactive Discussion



4 Discussion

4.1 Heat loss from the AW in the SAT: causes

Expanding on the AW circulation scheme suggested by Rudels et al. (2004) (Fig. 1), we have demonstrated that a significant portion of the heat associated with the SFSBW in the SAT disappears en route through the SAT. In this context, our observations confirm earlier findings by Hanzlick and Aagaard (1980). This concept, however, requires explanation for the AW intermediate temperature maximum of 2.74°C observed in the central SAT at 82°N (st. 80) that exceeds the temperature of the SFSBW inflow and outflow by 0.2°C and 0.65°C , respectively (Fig. 4a–b).

The current view on the AW circulation in the Eurasian Basin, as proposed by Rudels et al. (2004), implies that the FSBW could potentially feed all three temperature maximums along 82°N . However, the formation of each maximum is due to different FSBW branches. That is, if the SAT on-slope temperature maximums are associated with SFSBW, then the AW temperature maximum in the central SAT could be attributed to the boundary current of the FSBW flowing along the Siberian continental slope (yellow arrows in Fig. 2). The double diffusive staircases noticeable in st. 80 (Fig. 4b) provide evidence for attributing the intermediate temperature maximum of 2.74°C to the core of the FSBW that follows the Siberian continental slope rather than to the SFSBW. In contrast to the SFSBW inflow (sts. 23 and 85), CTD profiles taken in the SFSBW outflow (sts. 25 and 77) show heavily eroded double diffusive staircases (Fig. 4a and b). The SAT outflow also exhibits strong modification at the upper AW interface that is likely caused by vertical mixing and interaction with cooler and fresher surface water of Barents Sea origin. In contrast, the temperature and salinity profiles in the central SAT (st. 80) are only slightly modified at the upper AW interface and maintain double diffusive staircases that are almost disrupted in sts. 25 and 77 (Fig. 4a and b).

Usually, the enhanced turbulent diffusivity results in substantial degradation of the thermohaline staircases, and the turbulent mixing associated with shear instability nearly disrupts the double-diffusive staircases (e.g., Melling et al., 1984; Dmitrenko

OSD

11, 543–573, 2014

Heat loss from the Atlantic water layer

I. A. Dmitrenko et al.

Title Page

Abstract

Introduction

Conclusions

References

Tables

Figures

◀

▶

◀

▶

Back

Close

Full Screen / Esc

Printer-friendly Version

Interactive Discussion



Heat loss from the Atlantic water layer

I. A. Dmitrenko et al.

Title Page

Abstract

Introduction

Conclusions

References

Tables

Figures

◀

▶

◀

▶

Back

Close

Full Screen / Esc

Printer-friendly Version

Interactive Discussion



et al., 2008). Over the SAT eastern flank, turbulent mixing between the upper SFSBW and overlaying cooler and fresher Barents and Kara Sea water may be inferred from the velocity shear across the upper SFSBW interface (Figs. 6 and 7). The cross-trough potential density distribution in Fig. 5 is also consistent with a sheared geostrophic flow above the eastern SAT (Fig. 6a). Under this scenario, the SFSBW inflow (double-diffusive staircases present) has not been affected by enhanced turbulent mixing, while the SFSBW outflow (no double-diffusive staircases present) has experienced turbulent mixing during propagation along the eastern SAT. The FSBW boundary current at the central SAT (st. 80) has been partly affected by turbulent mixing, but double-diffusive staircases remain recognizable.

The sheared flow along the eastern SAT in the upper 100 m layer is evident from direct current observations (Fig. 6b), geostrophic velocity calculations (Fig. 6a), and model simulations (Figs. 6c, d and 7). However, the difference between measured and geostrophic velocities indicates that the SFSBW flow along the eastern SAT is not entirely density driven. In this context, Kirillov et al. (2012) recently showed that wind forcing over the northern Kara Sea is important in facilitating the SFSBW outflow from the SAT. The gradient Richardson number (Ri) provides a strong constraint for identifying turbulence produced by shear instability. It is defined as $Ri = N^2 S^{-2}$, where N is the Brunt–Vaisala frequency, and S is the flow vertical shear $S = [(dU/dz)^2 + (dV/dz)^2]^{1/2}$. Turbulent mixing can be assumed to occur for $Ri < 1$ (e.g., Polzin, 1996). Considering a velocity shear $S \sim 0.004 \text{ s}^{-1}$ and the stratification in the 30–90 m layer observed in 1996 (Figs. 5d and 6b) results in $Ri = 3.7$ which significantly exceeds the criterion. Simulations show, however, that velocity shear across the surface layer might reach 0.007 s^{-1} (Fig. 6d). Assuming the higher $S \sim 0.007 \text{ s}^{-1}$ induced by the SFSBW northward velocity $V \sim 40 \text{ cm s}^{-1}$, as measured in January 2010 (not shown), the $O(Ri) = 1.4$ might possibly allow for turbulent mixing, taking into account reduced salinity (density) stratification in winter due to sea-ice formation. While it cannot be shown explicitly that shear instability is entirely responsible for the enhanced vertical mixing, it may play a role in facilitating upward fluxes from the AW over the SAT eastern slope.

4.2 Heat loss from the AW in the SAT: estimates

In 2009, the heat content of the SFSBW inflow over the western SAT flank computed relative to the freezing temperature between 30 to 90 m depth decreased by $\sim 340 \text{ MJ m}^{-2}$ upon reaching the eastern flank. For example, at 81° N the heat content between 30 to 90 m depth decreased from 796 MJ m^{-2} at st. 23 (SFSBW inflow) to 457 MJ m^{-2} at st. 25 (SFSBW outflow). We note, however, the contrary tendency of the heat content over the eastern SAT between sts. 25 and 77, showing increase from 457 MJ m^{-2} at st. 25 to 584 MJ m^{-2} at st. 77 (Fig. 2). This discrepancy seems to be attributed to a crude spatial resolution of our time snapshot CTD data, which are insufficient to resolve the relatively narrow jet of the AW outflow from the SAT with horizontal temperature cross-slope gradients exceeding $1^\circ \text{ C}/10 \text{ km}$ (not shown).

In the following, we assume that all heat loss in the SFSBW occurs along the SAT eastern flank downstream of the SFSBW confluence with the Barents Sea water outflow to the SAT at $\sim 78^\circ \text{ N}$. This assumption is based on the hypotheses that the SFSBW heat loss is primarily driven by the velocity shear over the SAT eastern flank that is in line with model simulations showing no velocity shear over the SAT western flank (Fig. 7). This suggestion also implies neglecting the double diffusive heat loss from the AW over the SAT western flank, which is justified by the typical double diffusive heat flux estimated in the Arctic Ocean to 0.6 W m^{-2} (Sirevaag and Fer, 2012). Moreover, this assumption is also based on the structure of the temperature profiles, showing that the major part of the deepening of the upper SFSBW interface occurs from 81° N on the western flank to 81° N on the eastern flank (Fig. 4). Furthermore, we neglect the lateral heat loss, particularly by a fraction of the SFSBW flowing west along the shallower trough between Novaya Zemlya and Franz Josef Land – Fig. 1 (e.g., Schauer et al., 2002a; Gammelrød et al., 2009). The travel time along the eastern SAT flank between 78° N and the mooring location at 81° N is estimated using northward along-trough velocities simulated with the MIT model. At each grid node over the eastern flank, the simulated velocity profiles were averaged from 2003 to 2010 (Fig. 6c).

OSD

11, 543–573, 2014

Heat loss from the Atlantic water layer

I. A. Dmitrenko et al.

Title Page

Abstract

Introduction

Conclusions

References

Tables

Figures

◀

▶

◀

▶

Back

Close

Full Screen / Esc

Printer-friendly Version

Interactive Discussion



Heat loss from the Atlantic water layer

I. A. Dmitrenko et al.

Title Page

Abstract

Introduction

Conclusions

References

Tables

Figures

◀

▶

◀

▶

Back

Close

Full Screen / Esc

Printer-friendly Version

Interactive Discussion



The mean velocity profile computed from averaging all individual profiles over the eastern SAT shows $\sim 10 \text{ cm s}^{-1}$ northward velocity for the SFSBW core at $\sim 90 \text{ m}$ (Fig. 6c). This velocity implies a ~ 40 day travel time from 78° N to 81° N along the SAT eastern flank, the area where the heat content of the SFSBW was suggested to reduce by $\sim 340 \text{ MJ m}^{-2}$. This is equivalent to an upward vertical heat flux from the SFSBW to the low halocline water of $\sim 100 \text{ W m}^{-2}$. This rough estimate is similar to those reported by Sirevaag and Fer (2009) for the area north of Svalbard where the upward heat loss from the AW is among the largest throughout the Arctic Ocean (e.g., Steele and Morison, 1993). For comparison, over the Laptev Sea continental margins, Polyakov et al. (2012) estimated the heat flux across the upper AW interface of $\sim 8 \text{ W m}^{-2}$. Microstructure measurements over the Laptev Sea continental shelf break reveal upward heat fluxes of 12 W m^{-2} (Lenn et al., 2011). Over the SAT eastern flank, our model simulations show a mean upward heat flux across the upper SFSBW interface with values in the range $30\text{--}50 \text{ W m}^{-2}$ (Fig. 8) that is about half or less the heat loss compared with estimates inferred from CTD observations in the SAT. This difference indicates that the double diffusive heat loss over the SAT western flank and the lateral heat loss might be also important. On the other hand, the model presents a large spatial and temporal variability in the vertical heat fluxes at the upper SFSBW interface, with values at times exceeding 100 W m^{-2} . Therefore the inconsistency to the observations might be, in part, attributed to unresolved temporal variability. An incomplete model's mixing scheme might also provide an explanation for model-observational discrepancies.

4.3 Heat loss from the AW in the SAT: impact on sea ice

In what follows we test our hypothesis of enhanced SFSBW heat loss in the SAT by using sea-ice remote sensing data. The fraction of the AW heat expended for heating the overlaying water depends on the characteristics of the Barents Sea outflow. However, any upward heat flux reaching the sea surface will eventually affect the ocean–sea ice–atmosphere interface (e.g., through reduced sea-ice thickness, enthalpy flux to the atmosphere and delayed freeze-up). The winter mean (February–March) sea-ice

Heat loss from the Atlantic water layer

I. A. Dmitrenko et al.

Title Page

Abstract

Introduction

Conclusions

References

Tables

Figures

◀

▶

◀

▶

Back

Close

Full Screen / Esc

Printer-friendly Version

Interactive Discussion



thickness derived from five ICESat winter campaigns in 2004–2008 (Kwok et al., 2009) shows an area with negative anomalies of ~ 20 cm that stretches from the SAT mouth towards Severnaya Zemlya following the Nansen Basin continental margin (Fig. 9a). This is consistent with simulated velocity difference in Fig. 7 and enhanced upward heat loss along the SFSBW pathway (Fig. 8). In February–March 2004–2008, the ice drift over the SAT mouth is mainly westward with a mean velocity of ~ 4 km day $^{-1}$ (Fig. 9b and c). The mean width of the SAT eastern slope at the SAT mouth is ~ 50 km. This yields a ~ 12.5 days pack ice residence time over the SAT eastern slope at 82.5° N, where pack ice is exposed to the enhanced upward vertical heat flux from the SFSBW. The 20 cm sea-ice decrease in 12.5 days requires an upward heat flux of ~ 60 W m $^{-2}$ to the ice–water interface, which is similar to that obtained from the model simulations (Fig. 8).

The time series of ice concentration across SAT at 81° N reveals later freeze-up and earlier sea-ice decline at the eastern flank (73° E; mooring position), lagging the more western and eastern locations at 68° E and 78° E, respectively, by ~ 0.5 – 2.5 months (Fig. 10). This is in agreement with simulated sea-ice concentrations showing consistent reduction over the SAT eastern flank during freeze-up (October, contours in Fig. 7c) and melting (June, contours in Fig. 7d). For estimating the sea-ice growth during freeze-up, we use the semi-empirical method based on an analytical model known as the classical Stefan’s law (Stefan, 1891) that links the thermodynamic sea-ice growth to the cumulative surface air temperature below freezing. The accumulated sea-ice growth time series for 2005–2011 computed based on the surface air temperature from the NCEP reanalysis are shown in Fig. 11. For simplicity, we focus on satellite overpass times where the estimated thermodynamic sea-ice growth reaches ~ 20 cm, which roughly corresponds to the fall and winter sea-ice thickness anomaly over SAT in Figs. 7a and 9a, respectively. In contrast to the expected thermodynamic sea-ice growth of ~ 20 cm, the SAT eastern flank remains ice free even during the late fall at air temperatures far below freezing ($\sim -15^\circ$ C). For instance, on 25 October 2005 (Fig. 12a) the NCEP-derived daily mean air temperature was as low as -14° C, which

corresponds to a thermodynamic sea-ice growth of $\sim 2 \text{ cm day}^{-1}$ (Fig. 11). Melting this amount of ice requires $\sim 70 \text{ W m}^{-2}$ that approximately fits the upward heat flux inferred from the model simulation (Fig. 8). We note that this approach overestimates the heat loss because the Stefan's does not account for solar insolation.

The observed ice-free area, stretching along the SAT eastern flank (Fig. 12), is fully consistent with our assumption of a substantial AW heat loss along the eastern flank corroborated by a model simulation. Figure 12 is also in agreement with simulated sea ice thickness and concentration showing significant reduction over the SAT eastern flank in October (Fig. 7a and c). Another remarkable feature of sea ice in the SAT is that in 2005, 2007, 2008, 2009 and 2011 the area of reduced sea-ice concentration (45–85 %) was stretched along the SAT eastern flank further north to the SAT mouth at $\sim 82^\circ \text{ N}$ where it turned east following the Nansen Basin continental slope (e.g., Fig. 12c). This is also in line with (i) the spatial distribution of sea ice thickness anomaly in Fig. 9a and (ii) the enhanced AW heat loss simulated along the Kara Sea continental slope (Fig. 8).

The BSBW, entering the Arctic Ocean along the SAT, can also potentially impact the sea ice in this region (compare the BSBW pathway and configuration of the open water area in the SAT – Figs. 1 and 12). At the Barents Sea exit between Novaya Zemlya and Franz Josef Land, Årthun and Schrum (2010) simulated a long-term mean surface heat flux from the ocean of $\sim 10 \text{ W m}^{-2}$, which modifies the ice cover distribution as shown in Årthun et al. (2012). However, en route to the SAT, the warm core of the BSBW with temperatures above 0° and salinities between 34.8–35 psu is decoupled from the sea surface occupying the depths deeper than 70–100 m (Gammelsrød et al., 2009; Lien and Trofimov, 2013). Within the SAT, the warm BSBW core submerges even below the SFSBW (e.g., Dmitrenko et al., 2008, 2009). This suggests that the BSBW does not play a role in modifying the sea-ice conditions over the SAT through direct heat loss.

Heat loss from the Atlantic water layer

I. A. Dmitrenko et al.

Title Page

Abstract

Introduction

Conclusions

References

Tables

Figures

◀

▶

◀

▶

Back

Close

Full Screen / Esc

Printer-friendly Version

Interactive Discussion



5 Summary and concluding remarks

We have shown that the St. Anna Trough is one area of the Arctic Ocean where AW heat loss can modify the ocean–sea ice–atmosphere interface affecting both the formation and decay of sea ice. In this sense, the St. Anna Trough is generally similar to an “ice bay” known as Whalers’ Bay formed by inflowing Fram Strait branch of AW north of Svalbard (e.g., Ivanov et al., 2012). The sheared St. Anna Trough outflow to the Arctic Ocean is evident from shipboard ADCP as well as from geostrophic velocities and numerical model simulations. Although no clear evidence for the occurrence of shear instabilities could be obtained, we speculate that the enhanced upward heat flux in the St. Anna Trough is promoted by a vertical velocity shear along the St. Anna Trough eastern flank. We show that the zone of lowered sea ice thickness and concentration essentially marks the Fram Strait branch pathway in the St. Anna Trough and adjacent Nansen Basin continental margin from both sea-ice remote sensing observations and model simulations.

Our analysis was significantly limited by the availability of velocity data, and our heat flux estimates based on CTD observations were necessarily illustrative. Our cross-trough CTD transects are time snapshots, and the crude spatial resolution is insufficient to resolve the jet of the AW outflow from the St. Anna Trough. We also note that our estimates of the heat flux at the ice–water interface using sea-ice remote sensing show a lower bound because water and sea-ice dynamics are not taken into account. Moreover, we note that heat loss from the St. Anna Trough recirculating Fram Strait branch is not entirely available for sea-ice melt, and its important fraction is likely to be consumed for modifying the overlaying water and atmospheric boundary layer. We note that although Stephan’s law is a simplification of the requisite physics it does provide first-order agreement in our observed surface temperature fluxes and the thermodynamic response of the sea ice. Finally, the deficiencies of our analyses clearly define a necessity for further research in this area to quantify the efficiency of shear instability

OSD

11, 543–573, 2014

Heat loss from the Atlantic water layer

I. A. Dmitrenko et al.

Title Page

Abstract

Introduction

Conclusions

References

Tables

Figures

◀

▶

◀

▶

Back

Close

Full Screen / Esc

Printer-friendly Version

Interactive Discussion



in facilitating the heat loss from the St. Anna Trough recirculating Fram Strait branch involving advanced field experiments and further analyses of model simulations.

Acknowledgements. This study was supported by the Canada Excellence Research Chair (CERC) program and the Canada Research Chairs (CRC) program. The 2008–2010 oceanographic observations in the SAT were conducted under the working frame of the NABOS project with support from NOAA and NSF, the “System Laptev Sea” project funded through the German BMBF, and project “Arctika” (Russia). The numerical simulations were performed at the DKRZ, Hamburg, Germany in the frame of the German BMBF project “Nordatlantik” (WP 4.1) and the European Commission FP7 collaborative project “MONARCH-A” (FP7-Space-2009-1 contract 242446). We appreciate Lars Kaleschke (University of Hamburg, Germany) for providing the seaice concentration data through the Integrated Climate Data Center (ICDC) at the University of Hamburg, Germany. Yan Waddington and Torben Klägge have rendered valuable assistance in performing mooring deployment and recovery in the SAT.

References

- Årthun, M. and Schrum, C.: Ocean surface heat flux variability in the Barents Sea, *J. Marine Syst.*, 83, 88–98, 2010.
- Årthun, M., Eldevik, T., Smedsrud, L. H., Skagseth Ø., and Ingvaldsen, R. B.: Quantifying the influence of Atlantic heat on Barents Sea ice variability and retreat, *J. Climate*, 25, 4736–4743, 2012.
- Beszczynska-Möller, A., Fahrbach, E., Schauer, U., and Hansen, E.: Variability in Atlantic water temperature and transport at the entrance to the Arctic Ocean, 1997–2010, *ICES J. Mar. Sci.*, 69, 852–863, doi:10.1093/icesjms/fss056, 2012.
- Boyer, T., Levitus, S., Garcia, H., Locarnini, R. A., Stephens, C., and Antonov, J.: Objective analyses of annual, seasonal, and monthly temperature and salinity for the World Ocean on a 0.25° grid, *Int. J. Climatol.*, 25, 931–945, doi:10.1002/joc.1173, 2005.
- Dmitrenko, I. A., Kirillov, S. A., Ivanov, V. V., and Woodgate, R. A.: Mesoscale Atlantic water eddy off the Laptev Sea continental slope carries the signature of upstream interaction, *J. Geophys. Res.*, 113, C07005, doi:10.1029/2007JC004491, 2008.
- Dmitrenko, I. A., Bauch, D., Kirillov, S. A., Koldunov, N., Minnett, P. J., Ivanov, V. V., Hölemann, J. A., and Timokhov, L. A.: Barents Sea upstream events impact the properties of

OSD

11, 543–573, 2014

Heat loss from the Atlantic water layer

I. A. Dmitrenko et al.

Title Page

Abstract

Introduction

Conclusions

References

Tables

Figures

◀

▶

◀

▶

Back

Close

Full Screen / Esc

Printer-friendly Version

Interactive Discussion



Heat loss from the Atlantic water layer

I. A. Dmitrenko et al.

Title Page

Abstract

Introduction

Conclusions

References

Tables

Figures

◀

▶

◀

▶

Back

Close

Full Screen / Esc

Printer-friendly Version

Interactive Discussion



Atlantic water inflow into the Arctic Ocean: evidence from 2005–2006 downstream observations, *Deep-Sea Res.-Pt. I*, 56, 513–527, 2009.

Dmitrenko, I. A., Kirillov, S. A., Ivanov, V. V., Rudels, B., Serra, N., and Koldunov, N. V.: Modified halocline water over the Laptev Sea continental margin: historical data analysis, *J. Climate*, 25, 5556–5565, 2012.

Ezraty, R., Girard-Ardhuin, F., and Croizé-Fillon, D.: Sea ice drift in the central Arctic using the 89 GHz brightness temperatures of the advanced microwave scanning radiometer, *User's Manual*, IFREMER, Brest, France, 2007.

Gammelsrød, T., Leikvin, Ø., Lien, V., Budgell, W. P., Loeng, H., and Maslowski, W.: Mass and heat transports in the NE Barents Sea: observations and models, *J. Marine Syst.*, 75, 56–69, 2009.

Hanzlick, D. and Aagaard, K.: Freshwater and Atlantic Water in the Kara Sea, *J. Geophys. Res.*, 85, 4937–4942, 1980.

Ivanov, V. V., Alexeev, V. A., Repina, I., Koldunov, N. V., and Smirnov, A.: Tracing Atlantic water signature in the Arctic sea ice cover east of Svalbard, *Adv. Meteorol.*, 2012, 201818, doi:10.1155/2012/201818, 2012.

Kalnay, E., Kanamitsu, M., Kistler, R., Collins, W., Deaven, D., Gandin, L., Iredell, M., Saha, S., White, G., Woollen, J., Zhu, Y., Leetmaa, A., Reynolds, R., Chelliah, M., Ebisuzaki, W., Higgins, W., Janowiak, J., Mo, K. C., Ropelewski, C., Wang, J., Jenne, R., and Joseph, D.: The NCEP/NCAR 40 Year Reanalysis Project, *B. Am. Meteorol. Soc.*, 77, 437–471, 1996.

Kirillov, S. A., Dmitrenko, I. A., Ivanov, V. V., Aksenov, E. O., Makhotin, M. S., and de Quevas, B. A.: The influence of atmospheric circulation on the dynamics of the intermediate water layer in the eastern part of the St. Anna Trough, *Dokl. Earth Sci.*, 444, 630–633, 2012.

Kwok, R., Cunningham, G. F., Wensnahan, M., Rigor, I., Zwally, H. J., and Yi, D.: Thinning and volume loss of the Arctic Ocean sea ice cover: 2003–2008, *J. Geophys. Res.*, 114, C07005, doi:10.1029/2009JC005312, 2009.

Large, W. G., McWilliams, J., and Doney, S. C.: Ocean vertical mixing: a review and a model with a nonlocal boundary layer parameterization, *Rev. Geophys.*, 32, 363–403, 1994.

Lenn, Y. D., Rippeth, T. P., Old, C. P., Bacon, S., Polyakov, I., Ivanov, V., and Hölemann, J.: Intermittent intense turbulent mixing under ice in the Laptev Sea continental shelf, *J. Phys. Oceanogr.*, 41, 531–547, 2011.

Heat loss from the Atlantic water layer

I. A. Dmitrenko et al.

Title Page

Abstract

Introduction

Conclusions

References

Tables

Figures

◀

▶

◀

▶

Back

Close

Full Screen / Esc

Printer-friendly Version

Interactive Discussion



- Lien, V. S. and Trofimov, A. G.: Formation of Barents Sea Branch Water in the Northeastern Barents Sea, *Polar Res.*, 32, 18905, doi:10.3402/polar.v32i0.18905, 2013.
- Marshall, J., Adcroft, A., Hill, C., Perelman, L., and Heisey, C.: A finite-volume, incompressible Navier Stokes model for studies of the ocean on parallel computers, *J. Geophys. Res.*, 102, 5753–5766, 1997.
- Melling, H., Lake, R. A., Topham, D. R., and Fissel, D. B.: Oceanic thermal structure in the western Canadian Arctic, *Cont. Shelf Res.*, 3, 233–258, 1984.
- Polyakov, I. V., Timokhov, L. A., Alexeev, V. A., Bacon, S., Dmitrenko, I. A., Fortier, L., Frolov, I. E., Gascard, J.-C., Hansen, E., Ivanov, V. V., Laxon, S., Mauritzen, C., Perovich, D., Shimada, K., Simmons, H. L., Sokolov, V. T., Steele, M., and Toole, J.: Arctic Ocean warming contributes to reduced polar ice cap, *J. Phys. Oceanogr.*, 40, 2743–2756, 2010.
- Polyakov, I. V., Pnyushkov, A. V., Rember, R., Ivanov, V. V., Lenn, Y. D., Padman, L., and Carmack, E. C.: Mooring-based observations of double-diffusive staircases over the Laptev Sea slope, *J. Phys. Oceanogr.*, 42, 95–109, 2012.
- Polzin, K. L.: Statistics of the Richardson number: mixing models and fine structure, *J. Phys. Oceanogr.*, 26, 1409–1425, 1996.
- Rudels, B., Jones, E. P., Anderson, L. G., and Kattner, G.: On the intermediate depth waters of the Arctic Ocean, in: *The Polar Oceans and Their Role in Shaping the Global Environment: The Nansen Centennial Volume*, edited by: Johannessen, O. M., Muench, R. D., and Overland, J. E., *Geophys. Monogr. Ser.*, 85, AGU, Washington DC, 33–46, 1994.
- Schauer, U., Loeng, H., Rudels, B., Ozhigin, V. K., and Dieck, W.: Atlantic Water flow through the Barents and Kara Seas, *Deep-Sea Res.-Pt. I*, 49, 2281–2298, 2002a.
- Schauer, U., Rudels, B., Jones, E. P., Anderson, L. G., Muench, R. D., Björk, G., Swift, J. H., Ivanov, V., and Larsson, A.-M.: Confluence and redistribution of Atlantic water in the Nansen, Amundsen and Makarov basins, *Ann. Geophys.*, 20, 257–273, doi:10.5194/angeo-20-257-2002, 2002b.
- Serra, N., Käse, R., Köhl, A., Stammer, D., and Quadfasel, D.: On the low-frequency phase relation between the Denmark Strait and the Faroe-Shetland Channel dense overflows, *Tellus A*, 62, 530–550, 2010.
- Sirevaag, A. and Fer, I.: Early spring oceanic heat fluxes and mixing observed from drift stations north of Svalbard, *J. Phys. Oceanogr.*, 39, 3049–3069, 2009.
- Sirevaag, A. and Fer, I.: Vertical heat transfer in the Arctic Ocean: the role of double-diffusive mixing, *J. Geophys. Res.*, 117, C07010, doi:10.1029/2012JC007910, 2012.

- Skagseth, Ø.: Recirculation of Atlantic Water in the western Barents Sea, *Geophys. Res. Lett.*, 35, L11606, doi:10.1029/2008GL033785, 2008.
- Skagseth, Ø., Furevik, T., Ingvaldsen, R. B., Loeng, H., Mork, K. A., Orvik, K. A., and Ozhigin, V.: Volume and heat transports to the Arctic Ocean via the Norwegian and Barents Seas, in: Arctic Subarctic Ocean Fluxes: Defining the Role of the Northern Seas in Climate, edited by: Dickson, R., Meincke, J., and Rhines, P., Springer, New York, 45–64, 2008.
- 5 Spreen, G., Kaleschke, L., and Heygster, G.: Sea ice remote sensing using AMSR-E 89 GHz channels, *J. Geophys. Res.*, 113, C02S03, doi:10.1029/2005JC003384, 2008.
- Stefan, J.: Über die Theorie der Eisbildung, insbesondere über Eisbildung im Polarmeere, *Annalen der Physik und Chemie, Wiedemann-Annalen* 42, 269–286, 1891 (in German).
- 10 Steele, M. and Morison, J.: Hydrography and vertical fluxes of heat and salt northeast of Svalbard in autumn, *J. Geophys. Res.*, 98, 10013–10024, 1993.

Heat loss from the Atlantic water layer

I. A. Dmitrenko et al.

[Title Page](#)[Abstract](#)[Introduction](#)[Conclusions](#)[References](#)[Tables](#)[Figures](#)[◀](#)[▶](#)[◀](#)[▶](#)[Back](#)[Close](#)[Full Screen / Esc](#)[Printer-friendly Version](#)[Interactive Discussion](#)

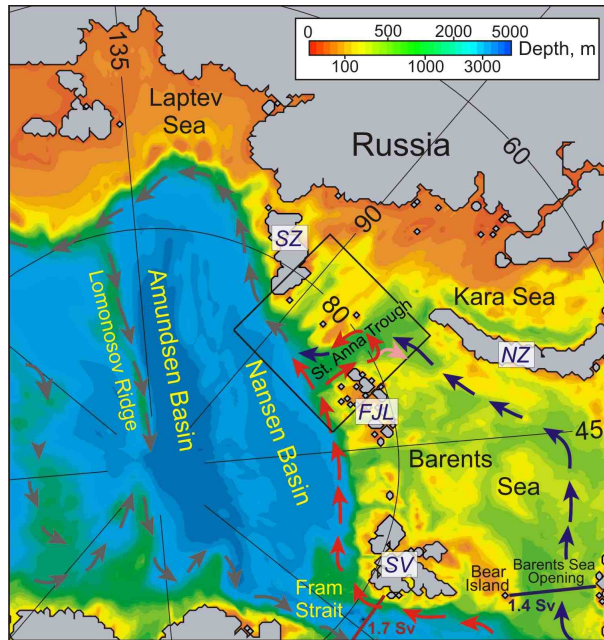


Fig. 1. Map of the inflow region of Atlantic Water (AW) to the Arctic Ocean. Arrows trace the Atlantic water (AW) pathways; red and blue arrows show the Fram Strait and Barents Sea branches, respectively, of the AW inflow into the Arctic Ocean in accordance with Rudels et al. (1994). The pink arrow shows a fraction of the Fram Strait branch water flowing west along the shallower trough between Novaya Zemlya and Franz Josef Land. Dark red and blue numbered lines in Fram Strait and Barents Sea Opening, respectively, show sections used for verifying the simulated volume transport of AW. Dark blue number indicates the simulated volume transport of AW (defined as $T > 3^{\circ}\text{C}$) through the Barents Sea Opening. Dark red number shows the simulated volume transport of AW (defined as $T > 2^{\circ}\text{C}$) in the core of the West Spitzbergen Current. The black rectangle encloses the region enlarged in Fig. 2. SV – Svalbard, FJL – Franz Josef Land, NZ – Novaya Zemlya, SZ – Severnaya Zemlya.

Heat loss from the Atlantic water layer

I. A. Dmitrenko et al.

Title Page	
Abstract	Introduction
Conclusions	References
Tables	Figures
◀	▶
◀	▶
Back	Close
Full Screen / Esc	
Printer-friendly Version	
Interactive Discussion	



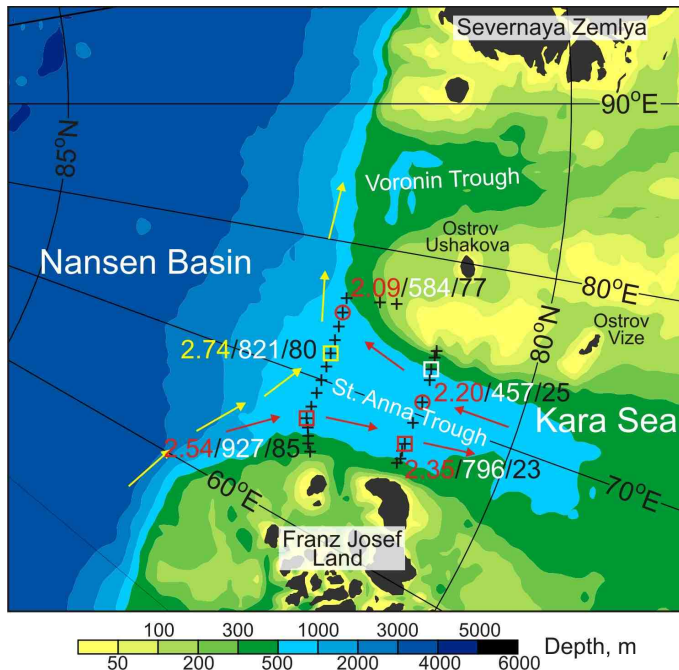


Fig. 2. A map of the northern Kara Sea with the St. Anna Trough (SAT). Arrows show the Fram Strait branch of the AW inflow into the Arctic Ocean that recirculates in the SAT (red arrows, SFSBW) and follows the continental margin (yellow arrows, FSBW). Crosses depict the positions of CTD stations taken in September 2009 at two sections crossing the SAT at $\sim 81^\circ$ N and 82° N. Red squares and circles identify stations taken through the core of the SFSBW inflow and outflow to/from the SAT, respectively. The yellow square identifies station taken through the core of the FSBW boundary current. The white square depicts mooring position. The first (yellow/red) number shows the FSBW/SFSBW core temperature ($^\circ\text{C}$) in September 2009. The second (white) number is heat content (MJ m^{-2}) computed relative to the freezing temperature between 30 to 90 m depth. The third (black) number denotes station number.

Heat loss from the Atlantic water layer

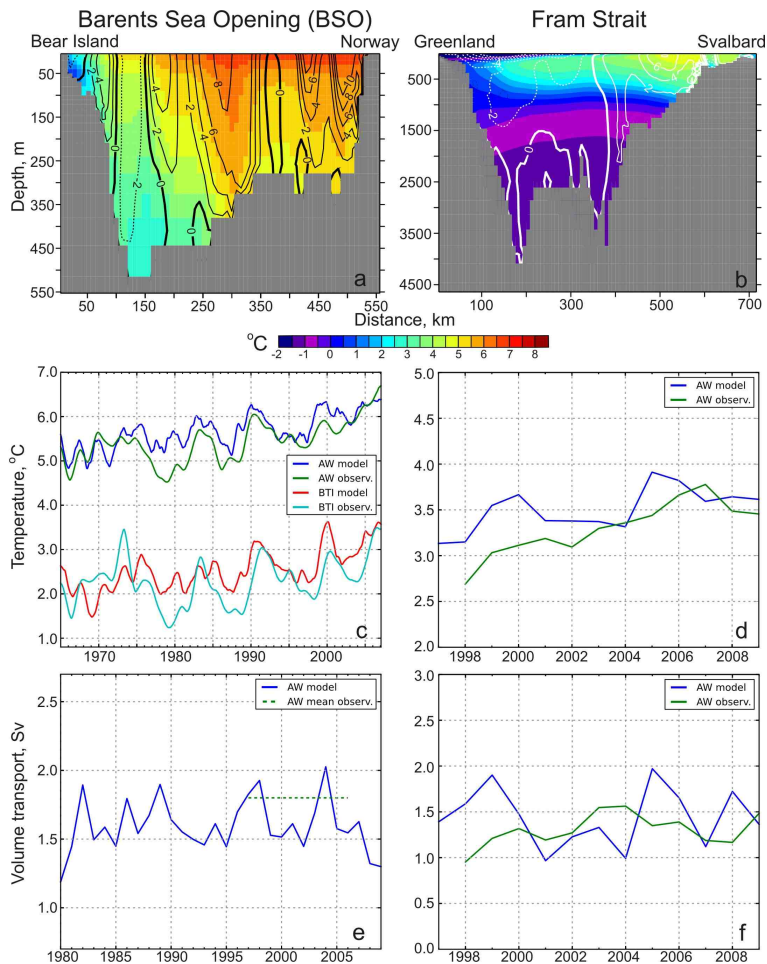
I. A. Dmitrenko et al.

Title Page	
Abstract	Introduction
Conclusions	References
Tables	Figures
◀	▶
◀	▶
Back	Close
Full Screen / Esc	
Printer-friendly Version	
Interactive Discussion	



Heat loss from the Atlantic water layer

I. A. Dmitrenko et al.



Title Page

Abstract

Introduction

Conclusions

References

Tables

Figures

◀

▶

◀

▶

Back

Close

Full Screen / Esc

Printer-friendly Version

Interactive Discussion



Heat loss from the Atlantic water layer

I. A. Dmitrenko et al.

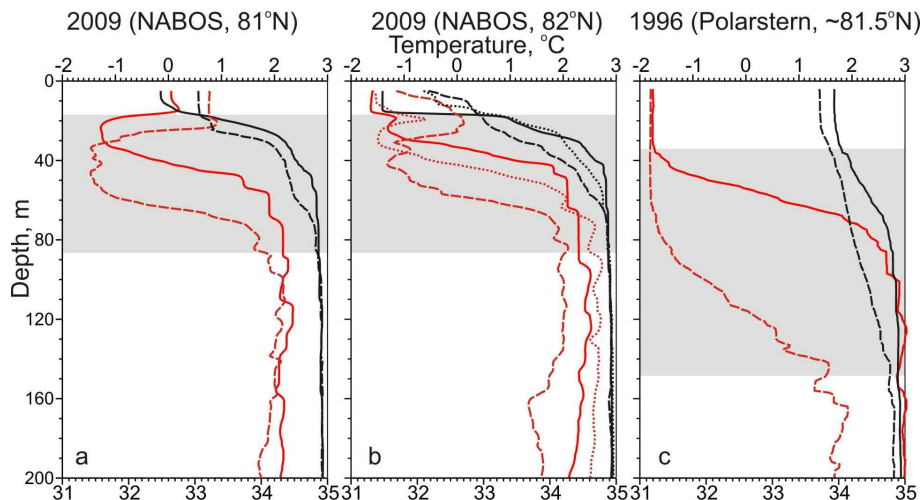


Fig. 4. Vertical profiles of temperature (red, °C) and salinity (black, psu) in the upper 200 m layer taken in July 1996 and September 2009 through the core of SFSBW inflow (solid line, left – st. 23, center – st. 85, right – $81^{\circ}27' \text{ N}$, $65^{\circ}51' \text{ E}$) and outflow (dashed line, left – st. 25, center – st. 77, right – $81^{\circ}17' \text{ N}$, $72^{\circ}01' \text{ E}$) to/from the SAT. **(b)** The dotted line depicts the CTD profile taken in September 2009 through the core of the FSBW boundary current (st. 80). For station positions in 2009 see Fig. 2. Gray shading highlights outflow from the SAT modified by vertical mixing.

Title Page

Abstract

Introduction

Conclusions

References

Tables

Figures

◀

▶

◀

▶

Back

Close

Full Screen / Esc

Printer-friendly Version

Interactive Discussion



Heat loss from the Atlantic water layer

I. A. Dmitrenko et al.

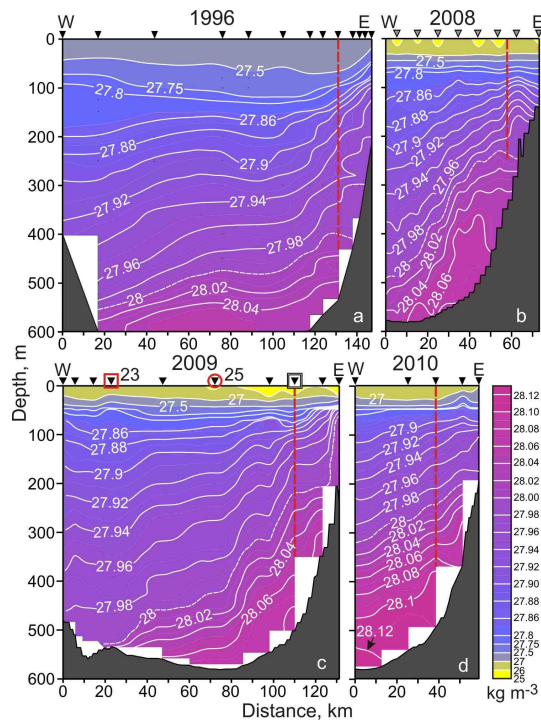


Fig. 5. 10 m binned cross-trough sections of potential density (σ -zero, kg m^{-3}) along 81°N for (a) July 1996, (b) September 2008, (c) September 2009 and (d) October 2010. Black and gray triangles on the top identify positions of CTD and XCTD stations, respectively. Following Fig. 2, the red square and circle and the white square identify stations taken through the core of the SFSBW inflow and outflow to/from the SAT and mooring position, respectively, with their reference numbers on the top. Red dashed lines identify locations of the geostrophic velocity profiles shown in Fig. 6a. The white dashed line highlights σ -zero = 28 kg m^{-3} that roughly corresponds to the core of the cooler fraction of BSBW (Dmitrenko et al., 2008, 2009).

Heat loss from the Atlantic water layer

I. A. Dmitrenko et al.

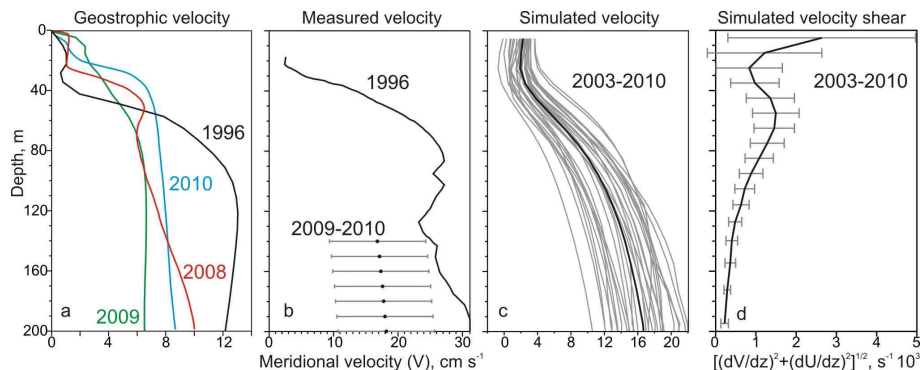


Fig. 6. Vertical velocity profiles for the northward current over the SAT eastern flank: **(a)** geostrophic, **(b)** measured and **(c)** simulated for each grid node over the SAT eastern flank between 78° N and 81° N (gray lines, averaged for 2003–2010 using annual mean velocity profiles) with their mean (black line). **(d)** Vertical profile of the simulated velocity shear at mooring position averaged for 2003–2010 using daily mean velocity profiles. **(b, d)** Error bars show one standard deviation of the mean.

Title Page

Abstract

Introduction

Conclusions

References

Tables

Figures

◀

▶

◀

▶

Back

Close

Full Screen / Esc

Printer-friendly Version

Interactive Discussion



Heat loss from the Atlantic water layer

I. A. Dmitrenko et al.

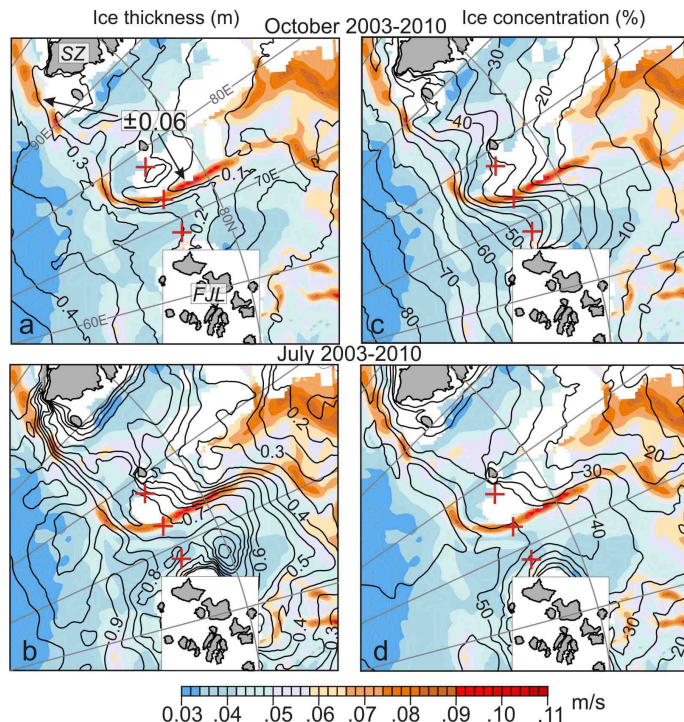


Fig. 7. The 7-year mean (2003–2010) simulated velocity difference (ΔV) in the 0–75 m layer (m s^{-1}) in the northern Kara Sea with overlaid simulated mean (**a**, **b**) sea-ice thickness (m) and (**c**, **d**) concentration (%) for (**a**, **c**) October and (**b**, **d**) July. Crosses depict locations along 81°N where the measured June–November time series of sea-ice concentration are compiled in Fig. 10. (**a**) Arrowed number shows \pm one standard deviation for the ΔV maximum over the SAT eastern flank and Kara Sea continental margin obtained using monthly mean velocity data.

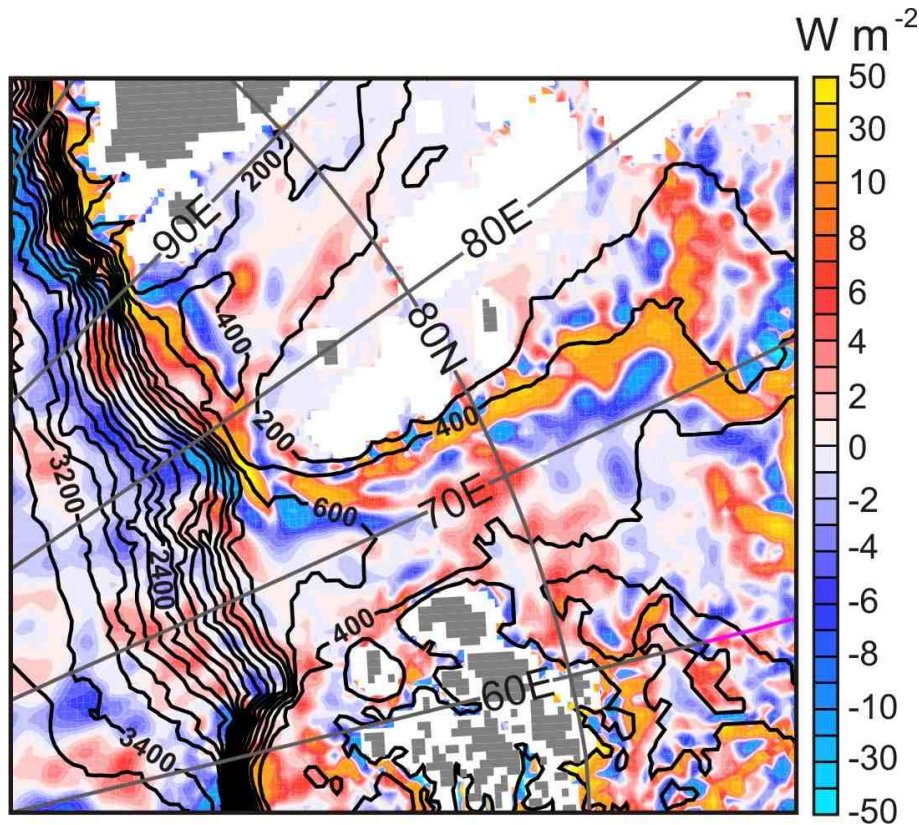


Fig. 8. The 7-year mean (2003–2010) simulated vertical heat fluxes (W m^{-2}) across the upper SFSBW interface at 75 m showing enhanced heat loss over the SAT eastern flank as well as over the Nansen Basin continental margin. Positive numbers indicate upward heat flux. The bathymetry is in meters.

Heat loss from the Atlantic water layer

I. A. Dmitrenko et al.

Title Page	
Abstract	Introduction
Conclusions	References
Tables	Figures
◀	▶
◀	▶
Back	Close
Full Screen / Esc	
Printer-friendly Version	
Interactive Discussion	



Heat loss from the Atlantic water layer

I. A. Dmitrenko et al.

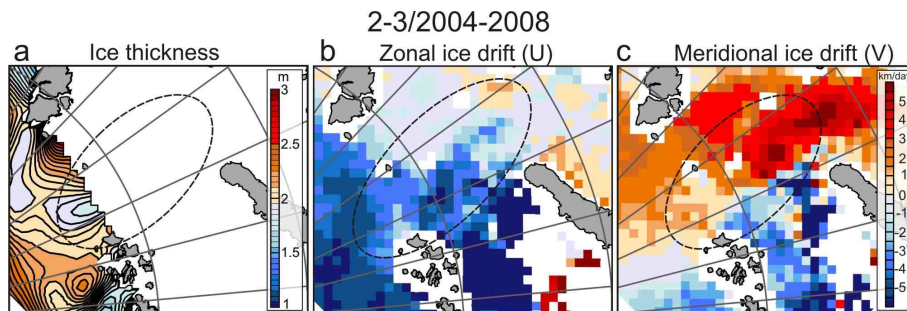


Fig. 9. The 2004–2008 winter mean (February–March) **(a)** seaice thickness (m) and **(b)** zonal and **(c)** meridional seaice drift (km day^{-1}) derived from AMSR data. The dashed oval highlights the SAT region.

[Title Page](#)[Abstract](#)[Introduction](#)[Conclusions](#)[References](#)[Tables](#)[Figures](#)[◀](#)[▶](#)[◀](#)[▶](#)[Back](#)[Close](#)[Full Screen / Esc](#)[Printer-friendly Version](#)[Interactive Discussion](#)

Heat loss from the Atlantic water layer

I. A. Dmitrenko et al.

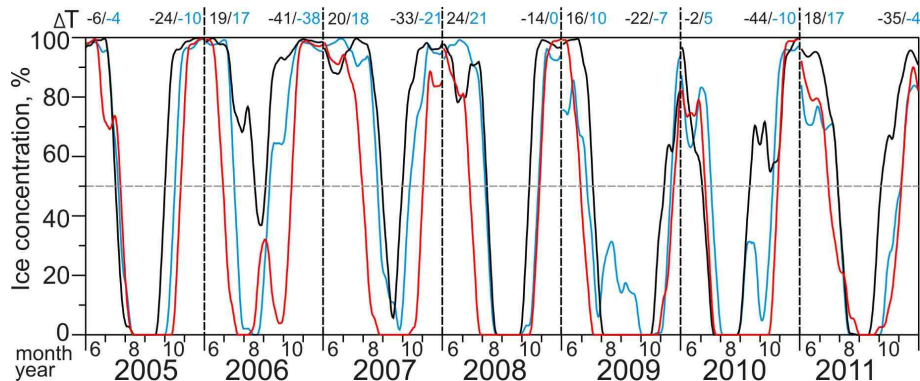


Fig. 10. The measured June–November time series of sea ice concentration (%) at three locations along 81° N depicted with crosses in Figs. 7 and 11a: 68° E (black), 73° E – mooring position (red), and 78° E (blue). Black/blue numbers at the top show the time lag (ΔT , days) between 73° E and 68° E/78° E on reaching the 50 % sea ice concentration.

Title Page

Abstract

Introduction

Conclusions

References

Tables

Figures

◀

▶

◀

▶

Back

Close

Full Screen / Esc

Printer-friendly Version

Interactive Discussion



Heat loss from the Atlantic water layer

I. A. Dmitrenko et al.

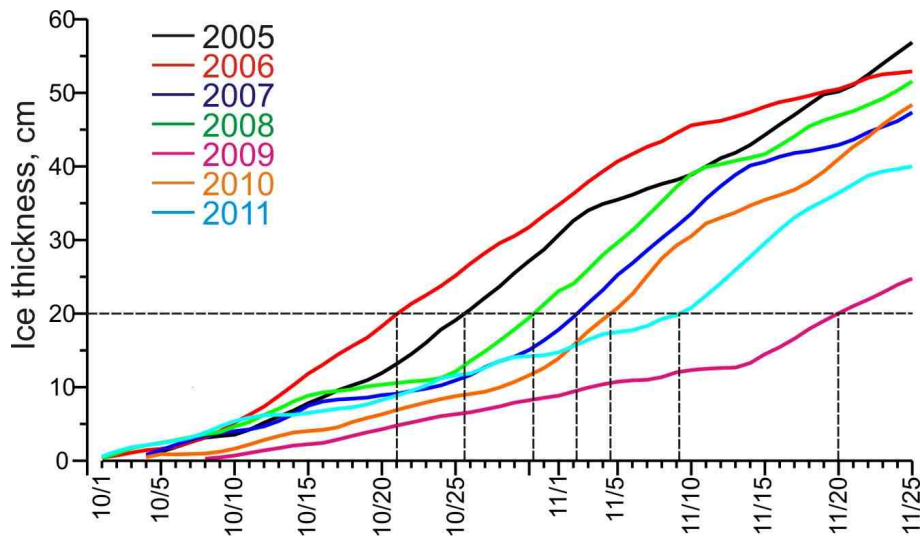


Fig. 11. Time series of accumulated thermodynamic seaice growth (cm) computed for October–November 2005–2011. Dashed lines indicate days in October–November when seaice thickness reached 20 cm.

[Title Page](#)[Abstract](#)[Introduction](#)[Conclusions](#)[References](#)[Tables](#)[Figures](#)[◀](#)[▶](#)[◀](#)[▶](#)[Back](#)[Close](#)[Full Screen / Esc](#)[Printer-friendly Version](#)[Interactive Discussion](#)

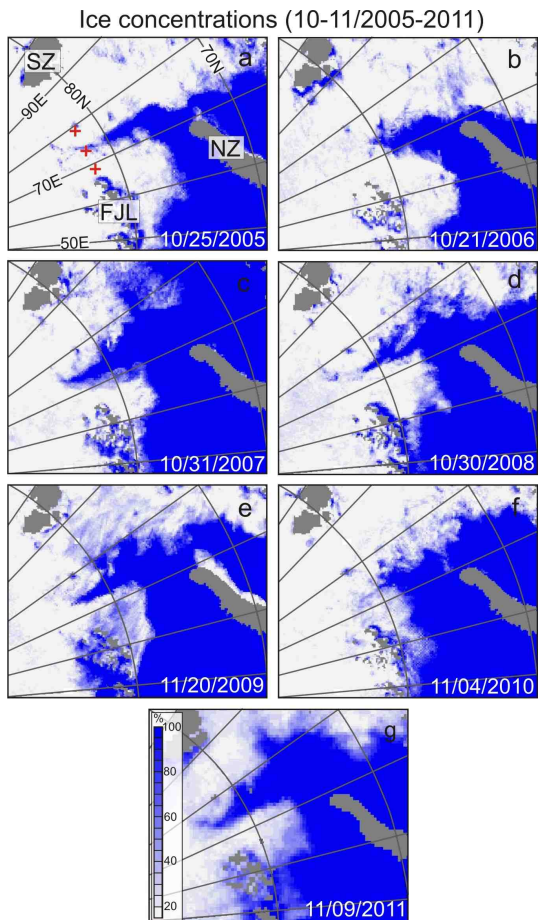


Fig. 12. (a–f) The AMSR-E and **(g)** SSMIS seaice concentrations (%) in October–November 2005–2011. Crosses in **(a)** depict locations along 81°N where the June–November time series of seaice concentration shown in Fig. 10 are compiled.